SCOSTEP
Scientific Committee on Solar-Terrestrial Physics

Variability of the Sun and Its Terrestrial Impact (VarSITI)
SEE / ISEST-Minimax24 / SPeCIMEN / ROSMIC
http://www.varsiti.org/

Vol. 20, December 2018

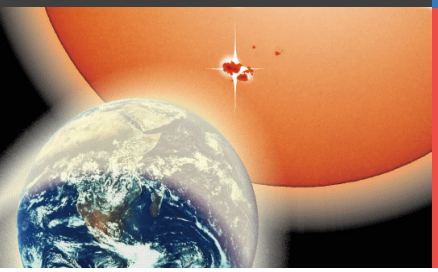

VarSITI Newsletter

Inside this issue

Project ROSMIC

Article 1:

Noctilucent Clouds and Climate Change

F.-J. Lübken, U. Berger, and G. Baumgarten
Leibniz Institute of Atmospheric Physics, Kühlungsborn, Germany

Franz-Josef Lüebken

Uwe Berger

Gerd Baumgarten

Noctilucent clouds (NLC) appear in the upper mesosphere (~83 km) during the summer season at middle and high latitudes. They consist of water ice particles which exist due to very low temperatures (<150 K). NLC were first reported in 1885, i. e., at the beginning of the industrial era. There is a long standing debate if NLC are a potential indicator of climate change. This relies on

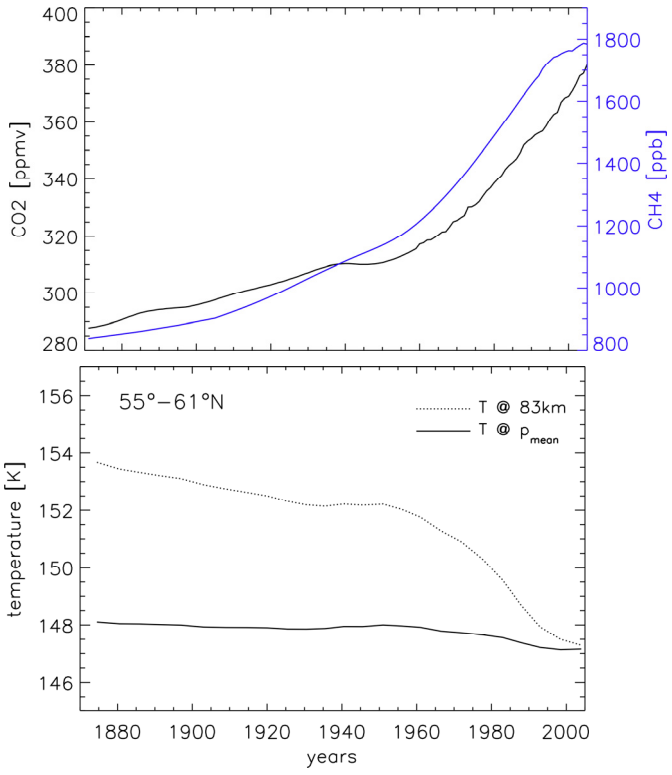

Figure 1. Upper panel: time series of tropospheric CO_2 (black) and CH_4 (green) mixing ratios. Lower panel: same, but for temperatures from run A at a fixed geometric altitude (83 km) and at the mean pressure level of maximum backscatter (p_{mean}). Data are averaged over solar cycles.

the simplified idea that an increase of greenhouse gases (here mainly CO_2) leads to a cooling of the middle atmosphere which should lead to more frequent and perhaps also more intense clouds. Indeed, observations and simulations covering the satellite era show non-significant trends (*DeLand and Thomas*, 2015; *Berger and Lübken*, 2015). Unfortunately, observations of basic atmospheric parameters in the mesosphere and lower thermosphere (MLT) relevant for NLC are not available for periods extending back to the preindustrial era.

The temporal evolution of NLC is complicated by the fact that several processes on time scales of decades interfere with long term trends, e. g., volcanic eruptions, and ozone decline/recovery. We have applied the MIMAS model (Mesospheric Ice Microphysics And tranSport model) to study trends in NLC on centennial time scales (1871 to 2008). In MIMAS several million dust particles are exposed to the background atmosphere and form ice particles, if conditions are favorable. From this we derive mean NLC parameters such as the maximum backscatter signal (β_{max}) as observed by lidars and ice water content (IWC). IWC gives the amount of water vapor bound in ice particles in a column of unit area and is frequently derived from satellite observations.

Background conditions for MIMAS are taken from the LIMA model (Leibniz Institute Model of the middle Atmosphere) which correctly represents the cold summer mesopause region. The concentrations of carbon dioxide (CO_2) and methane (CH_4) increase with time as shown in Fig. 1. We have performed three runs, namely A: increasing both carbon dioxide and methane ; B: increasing carbon dioxide, but keeping methane constant; C: increasing methane, but keeping carbon dioxide constant. Note that in the MLT nearly all methane is converted to water vapor which explains the similarity between methane and water vapor increase (not shown). As can be seen in Fig.1 temperatures in the latitude band 55°-61°N at a fixed altitude (83 km) decrease by roughly 7 K, whereas temperatures at a fixed pressure level in the same region are rather constant. This difference is explained by the so called 'shrinking effect' (see *Lübken et al.*, 2018, for more details). Note that the dynamical forcing of the MLT leading to the low summer MLT temperatures is kept constant in all runs.

The temporal development of the ice water content and maximum backscatter is shown in Fig. 2. IWC and β_{max} increase rapidly from preindustrial to modern times, but only if water vapor increase is considered (runs A and C). Surprisingly, an increase of carbon dioxide alone leads to a decrease(!) of β_{max} which can be explained by microphysical processes in the clouds.

In summary, some features of noctilucent clouds (e. g., IWC and β_{max}) are sensitive indicators of long term changes caused by anthropogenic increase of greenhouse gases, in particular water vapor. This applies mainly to centennial timescales because the morphology of NLC may be impacted by other processes on shorter periods, e. g., by ozone recovery.

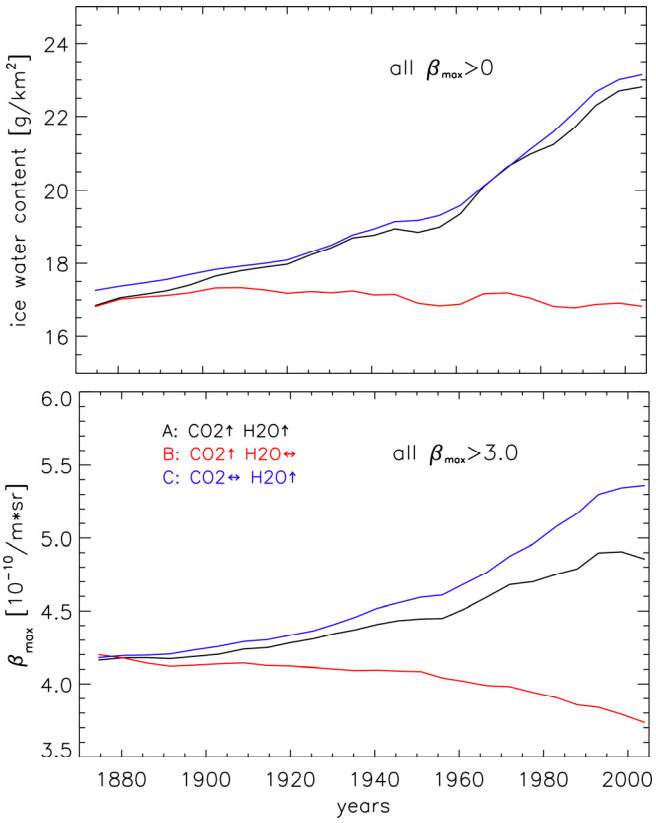

Figure 2. Upper panel: time series of ice water content in the latitude band 55-61°N for runs A (black), B (red), and C (green) where all β_{max}-values were considered. Lower panel: same but for maximum backscatter as observed by lidar. Only data with $\beta_{max}>3x10^{-10}$/m·sr were considered. Data are averaged over solar cycles.

References:

Berger, U., and F.-J. Lübken (2015), Trends in mesospheric ice layers in the Northern Hemisphere during 1961 - 2013, *J. Geophys. Res., 120*, 11,277–11,298, doi: 10.1002/2015JD023355.

DeLand, M. T., and G. E. Thomas (2015), Update PMC trends derived from SBUV data, *J. Geophys. Res., 120*, 2140–2166, doi:10.1002/2014JD022253.

Lübken, F.-J., U. Berger, and G. Baumgarten (2018), On the anthropogenic impact on long-term evolution of noctilucent clouds, *Geophys. Res. Lett., 45*, doi: 10.1029/2018GL077719.

Article 2:

Stable Auroral Red (SAR) Arc Observed at King George Island in 2017

C. M. Wrasse, C. A. O. B. Figueiredo, H. Takahashi, and J. V. Bageston
Instituto Nacional de Pesquisas Espaciais, INPE, São José dos Campos, SP, Brasil

Cristiano M. Wrasse | Cosme A. O. B. Figueiredo | Hisao Takahashi | Jose Valentin Bageston

During the geomagnetic storm event, May 27-28, 2017, a Stable Auroral Red (SAR) arc event was observed at Brazilian Antarctic Station (Comandante Ferraz), located at 62.1°S, 58.4°W (geomag lat: 52.2°S), King George Island, ~130 km North of the Antarctic Peninsula. The island is located under the middle latitude SAR-arc zone, but away from the auroral oval (Rees and Roble, 1975). This is the first time to catch the SAR-arc image from our observatory. Figure 1 shows the location of our observatory and the other airglow observation sites in the Antarctic Continent (ANGWIN - Antarctic Gravity Wave Instrument Network, https://www.scar.org/science/angwin/). The SAR-arc started to display at 02:40 UT (May 28) in the southern sky, and gradually moved toward the zenith, lasted up to 08:40 UT and disappeared in the northern sky. Figure 2 presents a snap shot of the OI 630 nm image at 03:39 UT. The image was taken by an airglow all-sky imager with a time integration of 90 seconds. The image was transformed to the geographic coordinates assuming the emission altitude to be around 250 km (airglow observation mode), and superposed on a map over the Antarctic Peninsula. One can notice that there are two bright band structures elongated in the east-west direction, one is a narrow band extending from 66° to 68°S, which must be the SAR-arc belt. The other one in the southern horizon (> 72°S) is much brighter and wide, showing a longitudinal structure. It looks to be a red aurora itself. Simultaneous OI 557.7 nm emission measurement did show an enhancement in the southern horizon, but no enhancement in the SAR-arc belt region. Two hours later the bright band structure gradually shifted toward north reaching over the King George island as shown in Figure 3 (a black dot indicates the location of observatory). It seems that the band shows a bright spot in the eastern side of horizon, suggesting a longitudinal gradient of the arc. Recent work by Mendillo et al. (2016) reported such a spatial variation of the arc. The temporal and spatial variations of the SAR-arc observed in the present case suggest us further investigation of SAR-arc in terms of the magnetosphere-ionosphere coupling.

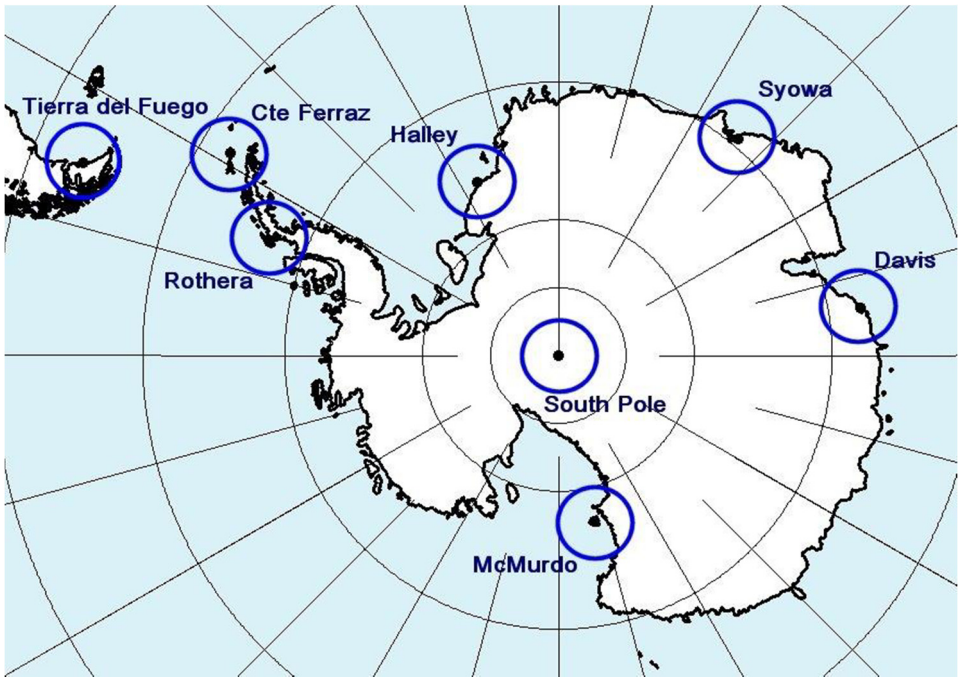

Figure 1. Gravity waves observatories at Antarctica Continent.
Source: http://www.inpe.br/angwin/pdf/presentation/01.pdf

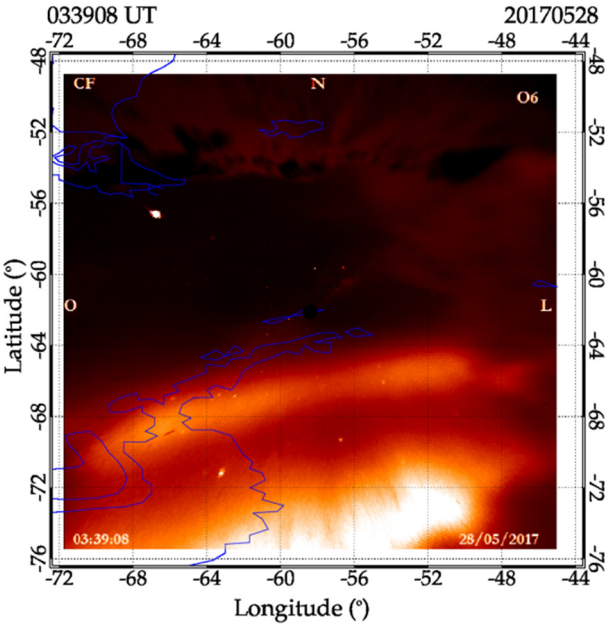

Figure 2. OI 630 nm image taken at Comandante Ferraz Station on May 28th at 03:39 UT. It is possible to see the SAR arc and Aurora. (The image was red color graded.)

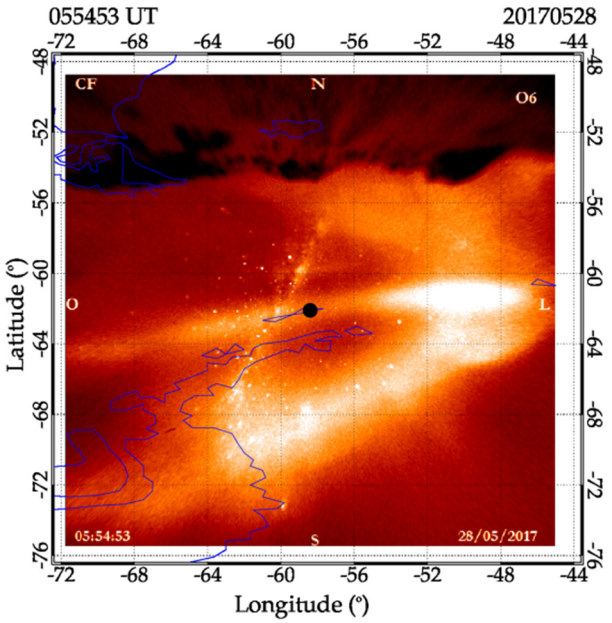

Figure 3. Same as Figure 2, except the image taken at 05:54 UT. It is possible to see the SAR arc and aurora activity shifted to North.

References:

Mendillo, M., J. Baumgardner, and J. Wroten (2016), SAR arcs we have seen: Evidence for variability in stable auroral red arcs, J. Geophys. Res. Space Physics, 121, 245–262, doi:10.1002/ 2015JA021722.

Rees, M. H., and R. G. Roble (1975), Observations and theory of the formation of stable auroral red arcs, Rev. Geophys. Space Physics, 13, 201–242, doi:10.1029/ RG013i001p00201.

Project SEE / ISEST

Article 3:

Database of Small-scale Magnetic Flux Ropes in the Solar Wind

Q. Hu and Y. Chen
Department of Space Science and CSPAR, The University of Alabama in Huntsville, Huntsville, AL, USA


Qiang Hu

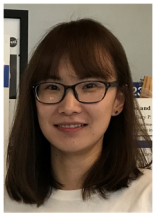
Yu Chen

Under the partial support of the VarSITI database development grant, a database of small-scale magnetic flux ropes (SSMFRs) in the solar wind detected by utilizing the Grad-Shafranov (GS) reconstruction technique has been built from Wind and ACE in-situ spacecraft measurements from year 1996 to 2017 (http://www.fluxrope.info/). Quantitative modeling and analysis of small-scale magnetic flux ropes from in-situ spacecraft measurements are essential for a better understanding of how they originate and interact with other solar wind structures. The detailed description of the methodology and analysis of detection results based on Wind spacecraft data are reported in Hu et al. (2018). A brief description of the methodology based on the GS reconstruction method including a *flowchart* illustrating the main procedures in the automated search algorithm are available on the database website.

Following Zheng and Hu [2018], the automated detection of small-scale magnetic flux ropes is implemented. Since the standard Grad-Shafranov equation guarantees that the transverse pressure P_t be a single-variable function of the magnetic flux function A, characterizing the cross section of a flux rope (Hu and Sonnerup, 2001, 2002) in this study, the detection of flux

ropes can be achieved by evaluating the double-folding pattern of the P_t versus A curve. First, we use multiple sliding windows of variable widths to search for possible flux ropes with different duration ranging from 9 minutes to about 6 hours. During the searching process, all spacecraft measurements are transformed to the quasi-static frame, i.e., usually the deHoffmann-Teller (HT) frame, in order to utilize the Grad-Shafranov equation which is based on the assumption of two-dimensional (2D) magnetohydrostatic equilibrium. After finding the new frame, we spilt the spacecraft path through a flux rope interval into two branches by determining the inflection point of the rotating field component. Values of P_t and A are calculated and two P_t versus A branches are compared to check if there exists double-folding pattern. The difference residue and the fitting residue are introduced to check the quality of this pattern. In addition, the Walén slope, representing the ratio of the remaining flow velocity to the local Alfvén velocity, is used to exclude the strong Alfvénic structures or waves. Lastly, the minimum value of average magnetic field magnitude is set at 5 nT to eliminate events contaminated by small fluctuations in the solar wind.

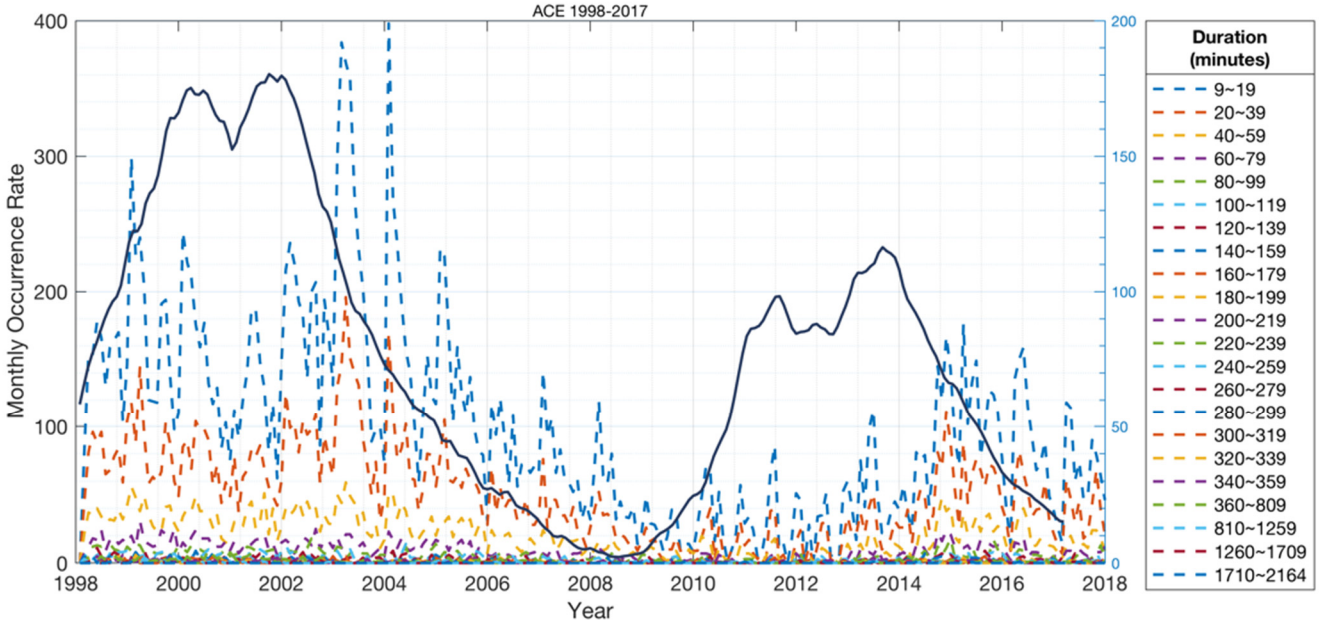

Figure 1. Monthly counts of occurrence of small-scale flux ropes from 1998 to 2017 for the ACE spacecraft. All dashed lines represent the counts of occurrence for each duration interval as denoted to the right. The solid curve is the monthly sunspot number.

The total number of small-scale flux ropes from our automated detection approach is 48,902 for the ACE in-situ spacecraft data. Among them, the total count of occurrence is 35,526 for the Solar Cycle 23 (1998 ~ December 2008) and 13,376 for the Solar Cycle 24 (December 2008 ~ 2017). Figure 1 indicates that the monthly count of small-scale flux ropes' occurrence follows the solar cycle, but usually peaks during the declining phase of each cycle. The intensity of solar cycle 23 and the total counts of small-scale flux ropes are greater than the solar cycle 24, which has the same trend as the Wind database result (Hu et al., 2018).

On the database website, the basic information of each small-scale flux rope event, containing time range, duration, residue, averaged parameters including the magnetic field, plasma beta, solar wind speed, and proton temperature, and orientation angles of flux rope axis are presented for each year. For every single event, graphic outputs including the curves of P_t versus A which can be used to check the double-folding quality, four hodograms for the magnetic field components, and plot of the Walén test are presented. In addition, plots of time-series magnetic field components, solar wind velocity and plasma parameters (beta, proton number density, temperature) are presented as well. Potential users of this database may contact the database developers for additional information. We acknowledge a number of NASA and NSF grants, and the VarSITI program for ongoing financial support.

Reference:

Hu, Q., Zheng, J., Chen, Y., le Roux, J., Zhao, L. 2018. Automated Detection of Small-scale Magnetic Flux Ropes in the Solar Wind: First Results from the Wind Spacecraft Measurements. The Astrophysical Journal Supplement Series 239, 12.

Project ROSMIC

Highlight on Young Scientists 1:

Investigation of Sporadic E-Layer in the Vicinity of Magnetic Dip Equator Using Satellite Radio Occultation and Ground-Based Measurements

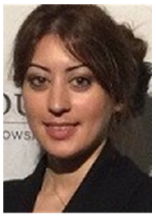

Aramesh Seif

Aramesh Seif
University of New Brunswick, Physics Department, Fredericton, New Brunswick, Canada

Sporadic E (*Es*) layers because of their strong vertical electron can cause intense disturbances in radio wave propagation. Knowledge of global *Es* properties and effects is of great interest to radio communications and navigations. Over the past decades, the identification of *Es* layers has been distinguished mostly from ground-based measurements including ionosondes (Whitehead, 1970). Recently, techniques for *Es* observations have remarkably enhanced. The GNSS radio occultation (RO) observa-

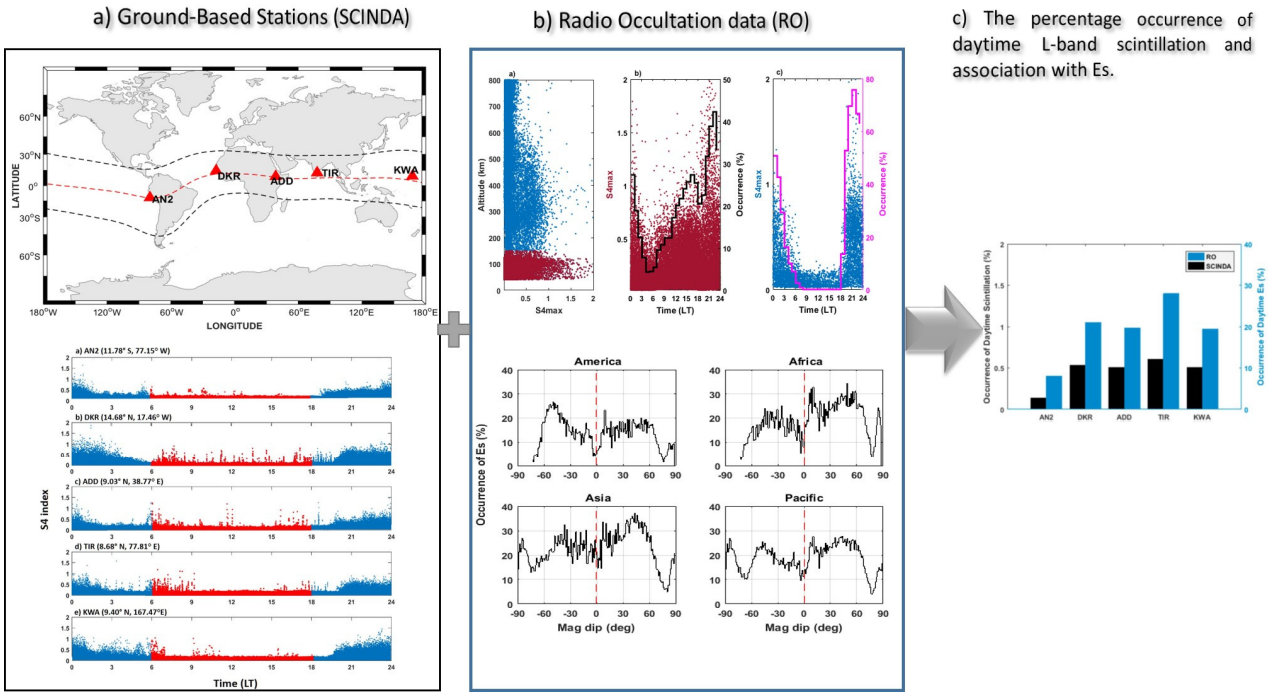

Figure 1a (first panel from above). Network of SCINDA stations situated near the magnetic dip equator. The red and black dashed curves denote the location of magnetic dip equator and the ±15° magnetic latitude, respectively. (1a second panel) Variations of daytime amplitude scintillation (S4 index) activities observed at five GNSS SCINDA stations (i.e., from above panel, at Ancon Dua (AN2), Dakar (DKR), Addis Ababa (ADD), Tirunelveli (TIR), and Kwajalein (KWA)) situated at the magnetic dip equator. The red points represent scintillation during daytime, and the blue points denote scintillation during nighttime.

Figure 1b. Amplitude scintillation statistics measured by FORMOSAT-3/COSMIC satellites in 2013. (1ba) Distributions of the scintillation as a function of altitude. (1bb) Distributions of the scintillation versus LT occurred at altitudes below 150 km (represented by red dots). (1bc) Distributions of the scintillation versus LT occurred at altitude above 150 km (represented by blue dots). The black (magenta) curve displays the percentage occurrence of Es in an altitude range below (above) 150 km.

Figure 1c. The percentage occurrence of daytime GHz scintillation and association with Es. Occurrences of Es with FORMOSAT-3/COSMIC RO data were measured from (±6°) of each station in longitude and latitude.

tion provides an ideal geometry with a significantly improved spatial and temporal vertical resolution, which has been used to study the *Es* layer structure (e.g., Wu et al., 2005; Arras et al., 2008; Seif et al., 2017; Zeng & Sokolovskiy, 2010).

We bring two data sets to bear, using the GNSS signal transmissions received on the ground- and from space, which provides a unique opportunity to retrieve complementary information about scintillation and association with *Es*. We present a comprehensive study of occurrence of GHz scintillation in association with the appearance of *Es* along the magnetic dip-equator during daytime (see Figure 1). Results for the first time show that daytime scintillation does occur along the magnetic dip-equator and the occurrence is associated with the appearance of *Es* observed using GNSS F3/C RO data. We show high (very low) occurrence of daytime scintillation in association with the *Es* was observed in the Asian (American) sector. In addition, we present the electric field and *Es* could act through the gradient-drift instability to produce irregularities that are responsible for GHz scintillations.

References:

Arras, C., J. Wickert, G. Beyerle, S. Heise, T. Schmidt, and C. Jacobi (2008), A global climatology of ionospheric irregularities derived from GPS radio occultation, Geophys. Res. Lett., 35, L14809, https://doi.org/10.1029/2008GL034158.

Seif, A., Liu, J.-Y., Mannucci, A. J., Carter, B. A., Norman, R., Caton, R. G., & Tsunoda, R. T. (2018), Equatorial Ionospheric Scintillation during Daytime, Eos, 99, https://doi.org/10.1029/2018EO106297.

Seif, A., Liu, J.-Y., Mannucci, A. J., Carter, B. A., Norman, R., Caton, R. G., & Tsunoda, R. T. (2017). A study of daytime L-band scintillation in association with sporadic E along the magnetic dip equator. Radio Science, 52. https://doi.org/10.1002/2017RS006393.

Seif, A., Tsunoda, R. T., Abdullah, M., & Hasbi, A. M. (2015). Daytime gigahertz scintillations near magnetic equator: Relationship to blanketing sporadic E and gradient-drift instability. Earth, Planets and Space Journal, 67(177), 1–13. https://doi.org/10.1186/s40623-015-0348-2.67:177.

Whitehead J. D. (1970) Production and prediction of sporadic E, Reviews of Geophysics 8:65.

Wu, D. L, C. O. Ao, G. A. Hajj, M. D. L. T. Juarez, A. J. Mannucci (2005), Sporadic E morphology from GPS-CHAMP radio occultation. J Geophys Res 110: A01306.

Zeng, Z., & Sokolovskiy, S. (2010). Effect of sporadic E clouds on GPS radio occultation signals. Geophysical Research Letters, 37, L18817. https://doi.org/10.1029/2010GL044561.

Highlight on Young Scientists 2:

Statistics of Coronal Dimmings Associated with Earth-directed CMEs


Karin Dissauer

Karin Dissauer
Institute of Physics, University of Graz, Graz, Austria

Coronal dimmings are localized regions of reduced emission in extreme-ultraviolet and soft X-rays (e.g. [1,2], see Fig. 1), that are formed due to density depletions occurring in the wake of CME eruptions in the low corona. Studying dimmings is essential to obtain additional information on the early evolution and characteristic parameters of Earth-directed CMEs, the main drivers of severe space weather disturbances affecting the near-Earth environment (e.g. [3]). This is of special interest as the characteristic properties of Earth-directed CMEs cannot be accurately measured due to strong projection effects.

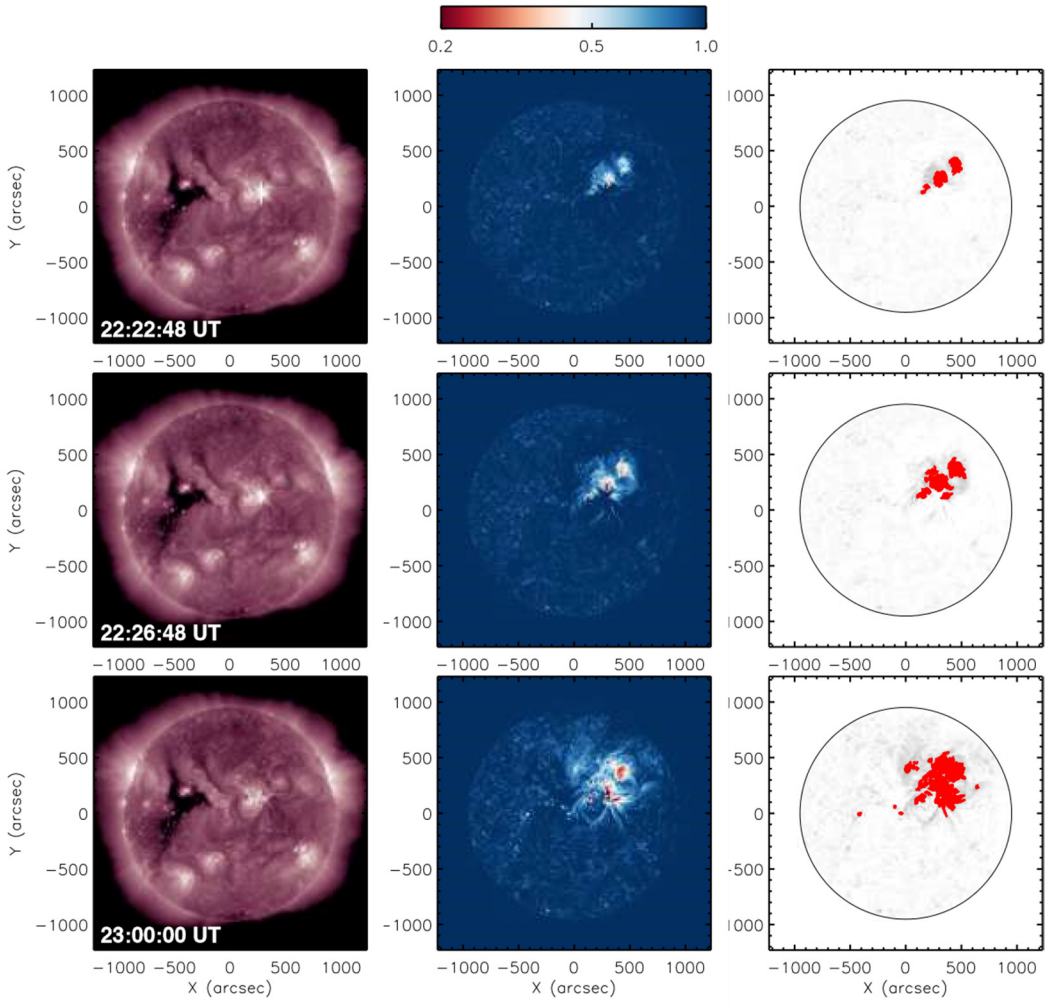

Figure 1. Sequence of SDO/AIA 211 Å direct (left) and logarithmic base-ratio images (middle) illustrating the expansion of the coronal dimming associated with the X2.1 flare/CME event on 2011 September 6. The right panels show the identified dimming pixels for each time step in red. Further details on the dimming detection method can be found in [4].

We recently investigated the statistical relationship between coronal dimmings, solar flares, and Earth-directed CMEs [5,6]. We found that parameters, describing the final extent of the dimming, such as its area, brightness and total magnetic flux strongly correlate with the flare fluence and the CME mass (c=0.6-0.7, Fig. 2 a). Parameters describing the dimming dynamics, such as the area growth rate, the brightness change rate and the magnetic flux change rate revealed a strong relationship with the flare strength and the maximal CME speed (c=0.6, Fig. 2 b).

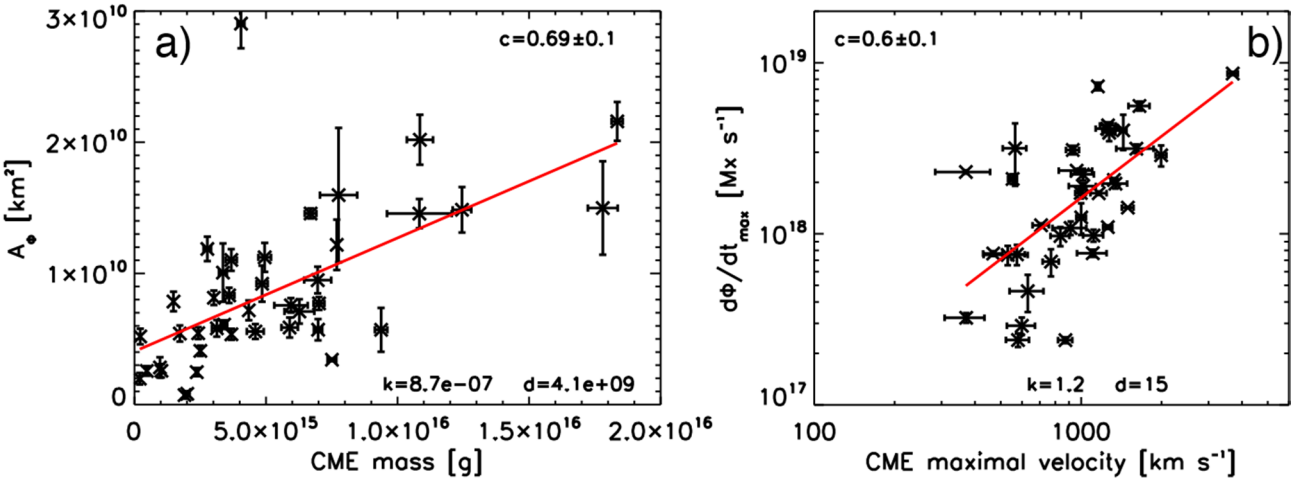

Figure 2. Left: Coronal dimming area against the CME mass in linear space. Right: Total unsigned magnetic flux change rate covered by the dimming region against the maximal speed of the CME in log-log space. The red line indicates the linear regression fit to all data points. The Pearson correlation coefficient is also given in each panel.

Our results imply that if CMEs occur together with flares, coronal dimmings statistically reflect the properties of both phenomena. In case of coronagraph failures EUV data would therefore give a tremendous support to retrieve information on Earth-directed CMEs.

References:

[1] Hudson, H. S., Acton, L.W., & Freeland, S. L. 1996, A Long-Duration Solar Flare with Mass Ejection and Global Consequences, Astrophys. J., 470, 629.

[2] Thompson, B. J., Plunkett, S. P., Gurman, J. B., Newmark, J.S., St. Cyr, O. C., Michels, D. J. 1998, SOHO/EIT observations of an Earth-directed coronal mass ejection on May 12, 1997, Geophys. Res. Lett., 25, 2465-2468.

[3] Gosling, J.T. 1993, The solar are myth, J. Geophys. Res., 98, 18937-18950.

[4] Dissauer, K., Veronig, A.M., Temmer, M., Podladchikova, T., Vanninathan, K., 2018, On the Detection of Coronal Dimmings and the Extraction of their Characteristic Properties, Astrophys. J., 855, 137.

[5] Dissauer, K., Veronig, A.M., Temmer, M., Podladchikova, T., Vanninathan, K. 2018, Statistics of Coronal Dimmings Associated with Coronal Mass Ejections. I. Characteristic Dimming Properties and Flare Association, Astrophys. J., 863, 169.

[6] Dissauer, K., Veronig, A.M., Temmer, M., Podladchikova, T. 2018, Statistics of Coronal Dimmings associated with Coronal Mass Ejections. II. Relationship between Coronal Dimmings and their Associated CMEs, Astrophys. J., submitted, arXiv: 1810.015189.

Project ISEST

Meeting Report 1:

ISEST 2018 Workshop

Bojan Vršnak
Hvar Observatory, Faculty of Geodesy, University of Zagreb, Zagreb, Croatia

Bojan Vršnak

Figure 1. Group photo of participants.

The "International Study of Earth-affecting Solar Transients ISEST 2018 Workshop", organized by Hvar Observatory, Faculty of Geodesy, University of Zagreb, was held from September 24 to 28, 2018 in the Hotel Amfora, Hvar, Croatia. The meeting was a concluding workshop of the ISEST project (http://solar.gmu.edu/heliophysics/index.php/ISEST).

More than 70 participants from 22 countries took part in ISEST 2018, presenting 41 oral presentations and 36 posters. The full Scientific Programme, including the Abstract Book and the List of Participants is available under the link "Abstract book" at http://oh.geof.unizg.hr/index.php/en/meetings/isest-2018.

The meeting was held under the auspices of the Hvar Town Council and Croatian Astronomical Society. The Colloquium was sponsored by the Ministry of Science and Education, Republic of Croatia, Scientific Committee on Solar Terrestrial Physics (SCOSTEP), VarSITI, International Association of Geomagnetism and Aeronomy (IAGA), and International Union of Geodesy and Geophysics (IUGG).

Project ROSMIC

Meeting Report 2:

The 15th International Symposium on Equatorial Aeronomy (ISEA-15) October 22 – 26, 2018, Ahmedabad, India

Duggirala Pallamraju
Chair, Scientific Organizing Committee & Convener, ISEA-15
Physical Research Laboratory, Ahmedabad, India

Duggirala Pallamraju

The 15th International Symposium on Equatorial Aeronomy (ISEA-15) was held at the Physical Research Laboratory (PRL), Ahmedabad, India during October 22 – 26, 2018. In all 249 abstracts accepted were distributed in the seven scientific themes in ISEA-15: Equatorial E- and F-region irregularities: Cause and effects; Longitudinal dependence of equatorial electrodynamics; Mesosphere Ionosphere Thermosphere coupling at low- and mid-latitudes; Mid- and low-latitude effects of global atmospheric wave coupling; Space weather effects on low- and mid-latitudes; Results from new techniques, experiments, and campaigns; and Future trends, opportunities, and challenges in low-latitude aeronomy. There were 64 oral presentations. All the posters were displayed on all the days which provided time for extended interactions. There were around 180 participants from 22 countries, with over 60 participants from out of India. A young scientist presentation competition was held wherein 43 young scientists participated. More information about the program, abstracts and other updates are available on the ISEA-15 website (https://www.prl.res.in/isea15).

Figure 1. Group photo of participants.

Meeting Report 3:

The 7th Brazilian Symposium on Space Geophysics and Aeronomy

José Valentin Bageston
Southern Regional Space Research Center, National Insitute for Space Research (CRS/INPE-MCTIC), Santa Maria, RS, Brazil

José Valentin Bageston

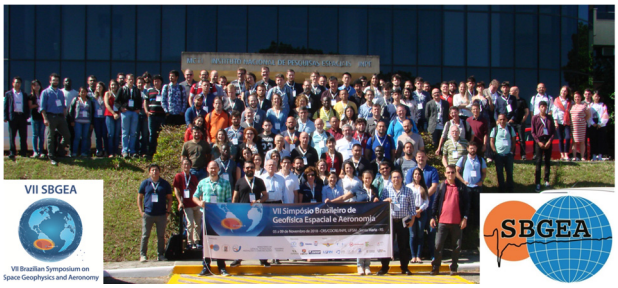

Figure 1. VII SBGEA Symposium official photo taken at CRS/INPE, Santa Maria-RS, on November 8, 2018.

The 7th SBGEA Symposium was held at the Southern Regional Space Research Center (CRS) of the Brazilian National Institute for Space Research (INPE) from 5 to 9 November 2018, in Santa Maria-RS, Southern Brazil. The Brazilian Space Geophysics and Aeronomy Association encourage and promote the achievement of this scientific event every two years. The scientific objective of this symposium was to show results of observational, theoretical and modeling studies obtained in recent years that will allow a better understanding of the Space phenomena, with origin in the Sun and in the interplanetary medium, which affects the whole atmosphere and Earth's climate. The 7th SBGEA was organized in 8 scientific sessions, with 7 invited talks and 43 normal oral presentations, totalizing 50 oral talks, and about 130 poster presentations. This symposium was supported by VarSITI/SCOSTEP, SBGEA, CAPES, FAPESP, FAPERGS and CBJLSW/NSSC/CAS. The details of the symposium can be found at http://www.sbgea.org.br/en/vii-sbgea-2/.

Upcoming meetings related to VarSITI

Conference	Date	Location	Contact Information
Chapman Conference on "Scientific Challenges Pertaining to Forecasting Space Weather Including Extremes"	Feb. 12-15, 2019	California, USA	https://chapman.agu.org/
2019 URSI Asia-Pacific Radio Science Conference (AP-RASC 2019)	Mar. 9-15, 2019	New Delhi, India	http://aprasc2019.com/
EGU General Assembly 2019	Apr. 7-12, 2019	Vienna, Austria	https://egu2019.eu/home.html
Japan Geoscience Union Meeting 2019 (JpGU)	May 26-30, 2019	Chiba, Japan	http://www.jpgu.org/en/index.html
VarSITI Completion Symposium	Jun. 10-14, 2019	Sofia, Bulgaria	http://www.varsiti.org/
27th IUGG General Assembly	Jul. 8-18, 2019	Montreal, Canada	http://iugg2019montreal.com/
AOGS 2019 16th Annual Meeting	Jul. 28-Aug.2, 2019	Singapore	http://www.asiaoceania.org/society/index.asp

The purpose of the VarSITI newsletter is to promote communication among scientists related to the four VarSITI Projects (SEE, ISEST/MiniMax24, SPeCIMEN, and ROSMIC).

The editors would like to ask you to submit the following articles to the VarSITI newsletter.

Our newsletter has five categories of the articles:

1. Articles— Each article has a maximum of 500 words length and four figures/photos (at least two figures/photos).
   With the writer's approval, the small face photo will be also added.
   On campaign, ground observations, satellite observations, modeling, etc.
2. Meeting reports—Each meeting report has a maximum of 150 words length and one photo from the meeting.
   With the writer's approval, the small face photo will be also added.
   On workshop/conference/ symposium report related to VarSITI
3. Highlights on young scientists— Each highlight has a maximum of 200 words length and two figures.
   With the writer's approval, the small face photo will be also added.
   On the young scientist's own work related to VarSITI
4. Short news— Each short news has a maximum of 100 words length.
   Announcements of campaign, workshop, etc.
5. Meeting schedule

Category 3 (Highlights on young scientists) helps both young scientists and VarSITI members to know each other. Please contact the editors if you know any recommended young scientists who are willing to write an article on this category.

TO SUBMIT AN ARTICLE

Articles/figures/photos can be emailed to the Newsletter Secretary, Ms. Ayumi Asai (a-asai_at_isee.nagoya-u.ac.jp). If you have any questions or problem, please do not hesitate to ask us.

SUBSCRIPTION - VarSITI MAILING LIST

The PDF version of the VarSITI Newsletter is distributed through the VarSITI mailing list. The mailing list is created for each of the four Projects with an integrated list for all Projects. If you want to be included in the mailing list to receive future information of VarSITI, please send e-mail to "a-asai_at_isee.nagoya-u.ac.jp" (replace "_at_" by "@") with your full name, country, e-mail address to be included, and the name of the Project you are interested.

Editors:

Kazuo Shiokawa (shiokawa_at_nagoya-u.jp)
Center for International Collaborative Research (CICR),
Institute for Space-Earth Environmental Research (ISEE), Nagoya University,
Nagoya, Japan
Tel: +81-52-747-6419, Fax: +81-52-747-6323

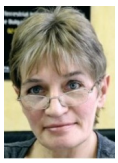

Katya Georgieva (kgeorg_at_bas.bg)
Space Research and Technologies Institute, Bulgarian Academy of Sciences,
Sofia, Bulgaria
Tel: +359-2-979-23-28

Newsletter Secretary:

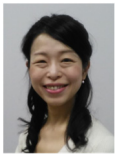

Ayumi Asai (a-asai_at_isee.nagoya-u.ac.jp)
Center for International Collaborative Research (CICR),
Institute for Space-Earth Environmental Research (ISEE), Nagoya University,
Nagoya, Japan
Tel: +81-52-747-6349, Fax: +81-52-789-5891

VarSITI Project co-leaders:

Piet Martens (SEE), Dibyendu Nandi (SEE), Vladimir Obridko (SEE), Nat Gopalswamy (ISEST/Minimax24), Manuela Temmer (ISEST/Minimax24), Jie Zhang (ISEST/Minimax24), Jacob Bortnik (SPeCIMEN), Craig Rodger (SPeCIMEN), Shri Kanekal (SPeCIMEN), Yoshizumi Miyoshi (SPeCIMEN), Franz-Josef Lübken (ROSMIC), Annika Seppälä (ROSMIC), and William Ward (ROSMIC)

SCOSTEP Bureau:

Nat Gopalswamy (President), Franz-Josef Lübken (Vice President), Marianna Shepherd (Scientific Secretary), Vladimir Kuznetsov（IUGG/IAGA), Mark Lester (IUPAP), Takuji Nakamura (COSPAR), Annika Seppälä (SCAR), Craig Rodger (URSI), Dan Marsh (IAMAS), Kyung-suk Cho（IAU)
web site: www.yorku.ca/scostep